Quaternary Science Reviews 321 (2023) 108367

Contents lists available at ScienceDirect

Quaternary Science Reviews

journal homepage: www.elsevier.com/locate/quascirev

Changes in climate extremes in Zambia during green and dry Sahara periods and their potential impacts on hominid dispersal

Francesco S.R. Pausata [a,*], Dominic Alain [a], Roberto Ingrosso [a], Katja Winger [a], Michelle S.M. Drapeau [b], Ariane Burke [b]

[a] Centre ESCER (Étude et la Simulation du Climat à l'Échelle Régionale) and GEOTOP (Research Center on the Dynamics of the Earth System), Department of Earth and Atmospheric Sciences, University of Quebec in Montreal, Montreal, QC, H2L 2C4, Canada
[b] Université de Montréal, Montreal, QC, H3T 1J4, Canada

ARTICLE INFO

Handling Editor: Dr Giovanni Zanchetta

Keywords:
Green Sahara
Zambia
Climate extremes
Hominid dispersal

ABSTRACT

Northern Africa experienced humid periods known as African humid periods or Green Sahara periods during the late Pleistocene and Holocene. The waxing and waning of the African Monsoon over the last several million years raises the question of how the climatic variability in the African Saharan region could have influenced the evolution and dispersion of hominins in Africa. Little is yet known about the changes in climate extremes in central southern Africa associated with these cycles and their potential impacts on human migration. In this study, we use a regional climate model to simulate archetypal Green and Desert Sahara periods under high and low boreal summer insolation and investigate the resulting changes in climate variability and extremes in South Tropical Africa, with a focus on Zambia. Our results indicate drier and warmer conditions under Green Sahara conditions relative to the Dry Sahara periods. In particular, an increase in the length of droughts and higher temperature extremes have been simulated over the Zambian region in the Green Sahara experiment. Our results suggest that during the Dry Sahara periods, Zambia may have offered better environmental conditions for hominin populations than the Central African Plateau (CAP). In contrast, the Green Sahara periods offered opposite conditions, potentially encouraging hominins to disperse through the large river valleys into the CAP and northward into the Sahel and Sahara.

All authors made substantial contributions to the submission. Francesco S.R. Pausata and Ariane Burke conceive the study. Dominic Alain and Roberto Ingrosso analyzed the model data. Katja Winger performed the model simulations. Francesco S.R. Pausata and Dominic Alain wrote the first draft of the manuscript.

1. Introduction

Recent archaeological and paleontological evidence suggests a complex, pan-African origin for our species, *Homo sapiens*, in which Sub-Saharan Africa (SSA) played a key role (Hublin et al., 2017; Klein and Richard Klein, 2019; Scerri, 2017; Stringer and Galway-Witham, 2017; Wilkins, 2021). Past climate variability in SSA, and specifically in South Tropical Africa, is believed to have influenced human population dynamics and evolution at the scale of the African continent (Blome et al., 2012; John E. Kutzbach et al., 2020)

The central plateau in the SSA is drained by the Zambezi, the third largest hydrological network on the African continent. This drainage system is considered by archaeologists to be an important biogeographic corridor, potentially influencing the pattern of hominin occupation of the region during the Stone Age with potential repercussions on human evolution in Africa (Larry Barham, 2000; Burrough et al., 2019; Colton et al., 2021).

Precipitation rates during the monsoon season exhibit large oscillations over a range of timescales, from interannual to interdecadal and longer periods (Fauchereau et al., 2003; Mason and Jury, 1997; Richard et al., 2001). On interannual timescales, for example, heavy rainfall can affect the region with daily precipitation locally exceeding 200 mm (Manhique et al., 2015) as well as prolonged droughts, such as the one in 1991–1992 (Vogel and Drummond, 1993). On longer timescales, the most notable climate shifts are the so-called African Humid Periods (AHPs), during which the West and East African Monsoon intensifies and the Intertropical Convergence Zone (ITCZ) is displaced northward, transforming the hyper-arid Sahara Desert into a mesic environment

* Corresponding author.
E-mail address: pausata.franscesco@uqam.ca (F.S.R. Pausata).

https://doi.org/10.1016/j.quascirev.2023.108367
Received 7 July 2023; Received in revised form 10 October 2023; Accepted 14 October 2023
Available online 3 November 2023

(deMenocal and Tierney, 2012; Gasse et al., 1990) and affecting the climate worldwide (Dandoy et al., 2021; Pausata et al., 2017a; 2017b; Pausata et al., 2021; Piao et al., 2020; Sun et al., 2019). The last AHP occurred between about 11000 and 5000 years ago (Castañeda et al., 2009; P. deMenocal et al., 2000; Gasse, 2000; Hély et al., 2014; Hoelzmann et al., 1998; Tierney et al., 2017; Yu and Harrison, 1996) and AHPs are a direct response of the African monsoon to the precession cycle, a periodic variation in Earth's orbit around the sun (Berger, 1978). During AHPs, the Earth is closer to the sun during boreal summer and farther away during boreal winter compared to today, which leads to warmer summers and colder winters in the Northern Hemisphere. The warmer summers in the Northern Hemisphere caused a northward extension of the Hadley circulation, which allowed the West African Monsoon (WAM) to penetrate further north (Gaetani et al., 2017; Kutzbach, 1981). The waxing and waning of the WAM over the last eight million years (Armstrong et al., 2023; Larrasoaña et al., 2013) may have impacted human evolution and dispersal throughout Africa thanks to pluvial corridors created in the Sahara region (Castañeda et al., 2009; Drake et al., 2011; Hublin et al., 2017; Osborne et al., 2008; Smith, 2012; Szabo et al., 1995). Researchers have recently proposed that our human lineage evolved on a continental scale, as climatic cycles reconnected populations in the ''cradle of humankind'' in South Africa with populations elsewhere in Africa (Hublin et al., 2017). The exact dispersal routes are still a subject of debate, but AHPs are thought to have influenced their development (Abbate and Sagri, 2012; Agustí and Lordkipanidze, 2011; Reynolds, 2015; Timmermann and Friedrich, 2016). A similar dynamic is suggested for the south tropical zone of Africa, where the Central Plateau and the Kalahari Desert cycled from arid to relatively humid conditions, potentially limiting the distribution of hominin populations and enhancing the importance of major watercourses such as the Zambezi as potential ''refugia'' (Burrough et al., 2019).

To our knowledge, no study has hitherto investigated the impact of AHPs in Tropical Africa south of the equator. The geographic position of this region, which lies between southern Africa and the East African Rift, where hominins likely first evolved, and northern Africa, where the most ancient proof of the existence of *Homo sapiens* is known (Hublin et al., 2017; Richter et al., 2017), means that this region is critical for our understanding of the dynamics of human biocultural evolution in Africa.

In this study, we use a regional climate model to simulate archetypal Green and Desert Sahara periods under high and low boreal summer insolation and investigate the changes in climate variability and extremes in southern Tropical Africa, focusing on its central region, Zambia. This research aims to shed light on the changes in precipitation and temperature variability, and extremes in the area associated with the waxing and waning of the WAM. These results may help constrain the impact of climate change on the course of human evolution and dispersal.

2. Materials and methods

2.1. Study area and its climate

SSA is dominated by a central plateau of more than 1 million km^2, bordered to the northeast by the Western Rift of Tanzania and Malawi, to the southeast by the Luangwa and Upper-Zambezi Rifts, and to the northwest by the Upemba Rift (Daly et al., 2020). The model domain covers the entire SSA (10°N - 35°S; 15°W – 55°E) (Fig. 1a) with a primary focus on Zambia (Fig. 1). Three areas within Zambia were chosen for more detailed analysis: Northeastern Zambia (10.82°S; 33.07°E), Central Luangwa River Valley (13.19°S; 31.71°E), and Zambia's capital city, Lusaka (15.42°S; 28.28°E). Lusaka is located at the southern end of the Central African Plateau (CAP). We chose the Central Luangwa River Valley because it forms part of the Zambezi watershed, a primary hydrological system that drains central Africa. Recent studies have highlighted archaeological evidence of hominin occupations in the area from the middle Pleistocene onwards, as well as evidence of critical climatic fluctuations (Barham et al., 2011; Burke et al., 2021; Colton et al., 2021). Central southern Africa is a region that lies in the tropics and experiences a monsoon climate with high annual and interannual rainfall variability (Fauchereau et al., 2003; Mason and Jury, 1997; Richard et al., 2001). At these timescales, three different contributions of surface airstreams influence the rainfall pattern in central southern Africa (Nicholson, 2019). Firstly, southeastern trade winds that originate over the Indian Ocean to the east and the south of Africa, as well as northeasterly monsoonal flow from the Indian subcontinent. All of them are thermally stable with subsiding dry air (Nicholson, 2019). Warm and humid easterly trade winds meet at the ITCZ. When the high insolation season in boreal summer occurs, the ITCZ moves northward toward the area of low pressure over the Sahara Desert and the dry southeast trades control the central southern Africa climate. On the contrary, in January, when the ITCZ is further south, heavy rain is expected in central southern Africa as the convergence zone moved southward (Nicholson, 2019). The third airstream is a westerly flow that comes from the South Atlantic Ocean and converges with the two latter easterly currents (Nicholson, 2019). The airstream flows across the Congo basin and cools to saturation due to the high elevation of eastern Africa, bringing heavy rain (Nicholson, 2019). The Southeastern Africa monsoon is associated with a period of heavy rainfall lasting from November to April with the precipitation peaking from December to February.

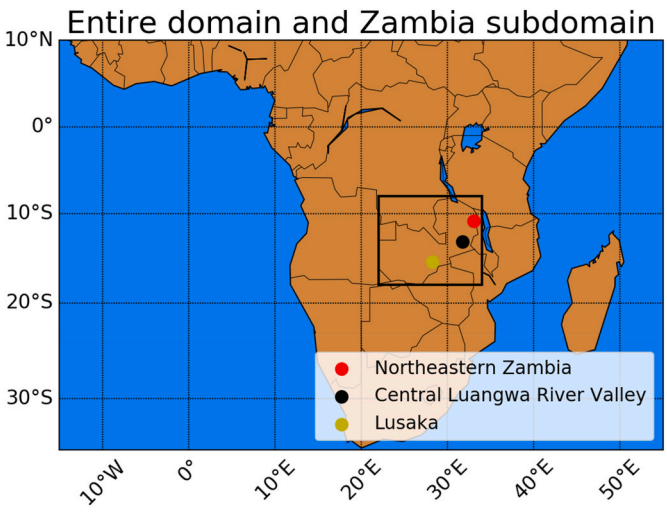

Fig. 1. Study area: entire regional climate model domain with the Zambia subdomain (black rectangle) as well as the three subregions more extensively discussed (colored dots).

2.2. Model description

The Regional Climate Model (RCM) employed in this study is the developmental version of the Canadian Regional Climate Model 5th generation (CRCM5) based on the Global Environment Multiscale 4 (GEM4) model (Girard et al., 2014; McTaggart-Cowan et al., 2019) developed by the Recherche en Prévision Numérique (RPN) and the Canadian Meteorological Centre (CMC). The subgrid-scale physical parameterizations include the Kain and Fritsch (1990) deep-convection and Kuo-transient (Kuo, 1965) shallow-convection schemes, as well as the large-scale condensation scheme (Sundquist et al., 1989), the correlated-K scheme for solar and terrestrial radiations (Li and Barker, 2005), a sub-grid scale mountain gravity-wave drag (McFarlane & A., 1987) and low-level orographic blocking (Zadra et al., 2010), a turbulent kinetic energy closure in the planetary boundary layer and vertical diffusion (Benoit et al., 1989; Delage, 1997; Delage and Girard, 1992), and a weak ∇^6 lateral diffusion. The land-surface scheme, however, is changed from the Interaction Sol-Biosphère-Atmosphère (ISBA) scheme

used at CMC for the Canadian LAnd Surface Scheme (CLASS) (Verseghy, 2000, 2010) to its most recent version, CLASS 3.6. For these simulations, 16 soil layers are used, reaching a depth of 10 m. The standard CLASS distributions of sand and clay fields, as well as the bare soil albedo values, are replaced with data from the ECOCLIMAP database (Masson et al., 2003). Finally, the interactive thermodynamic 1-D lake module (FLake model) is also used (Martynov et al., 2012).

2.3. Experimental design

We use model output from global simulations carried out by Gaetani et al. (2017) and Pausata et al. (2016) with an Earth System Model (EC-Earth version 3.1) at a horizontal resolution of 1.125° × 1.125° and 62 vertical levels for the atmosphere to drive regional simulations at the lateral and lower boundaries at a horizontal resolution of 0.11° (~12 km).

We carry out the following three simulations (Table 1 and 2): 1) the pre-industrial (PI) climate in which PI greenhouse gases (GHGs) and current vegetation cover are prescribed to represent the low insolation – dry Sahara case (LI_{DS}). The other two idealized simulations are performed under middle Holocene (MH) solar orbital forcing 6000 years ago. 2) With respect to the LI_{DS} simulation, we only change in the first MH sensitivity simulation the GHGs and the orbital forcing which are set as MH, following the Paleoclimate Intercomparison Project phase 3 (PMIP3) protocol (Taylor et al., 2009). The boundary conditions are the same as the for the LI_{DS} simulation. This experiment represents the high insolation – dry Sahara (HI_{DS}), i.e., a transition state at the end of the AHPs. 3) In the second MH experiment, the lower and lateral boundary conditions are changed as well, using output from a global model experiment in which the Saharan surface (11°–33°N, 15°W–35°E) was changed from desert to shrubs, and PI dust concentrations are reduced by up to 80% (for more details see Gaetani et al. (2017) and Pausata et al. (2016). This experiment represents the high insolation – green Sahara (HI_{GS}). Each simulation is 30 years long. The LI_{DS} is the reference simulation for desert Sahara conditions and low boreal summer insolation, while the HI_{GS} is the reference simulation for the green Sahara state and high boreal summer insolation. Daily maximum and minimum temperatures and precipitation are used to analyze the changes in climatology and climate extremes.

2.4. Climate extreme indices

Daily temperature and precipitation data are used to calculate extreme climate indices. Here, we use temperature and precipitation climate indices defined by the Expert Team on Climate Change Detection and Indices (ETCCDI) (Zhang et al., 2011). They defined a set of extreme climate indices based on temperature and precipitation. In this study, we examine the changes in selected indices for the 30 years of each simulation, as we display their spatial distribution over the entire SSA domain. From the 27 available indices in the ETCCDI, we selected the six most commonly used (Table 1.2). In particular, we chose the annual maximum daily maximum temperature or the hottest day of the year (TXx), the annual minimum daily minimum temperature or the coldest night of the year (TNn), and the number of tropical nights per year (TRn), that is, the number of nights in which the minimum temperature does not fall below 20 °C. We also considered the number of consecutive dry days (CDD) that constitutes the maximum number of consecutive days in a given year with precipitation less than 1 mm, that is, the longest dry spell of the year. The annual maximum precipitation amount fallen over five consecutive days (RX5day), which is used to identify prolonged heavy rainfall events, and the number of wet days per year in which the daily precipitation exceeds 1 mm (R1mm). The statistical significance of the changes was estimated based on the Student two-tailed *t-test* (Yuen and Dixon, 1973) and the non-parametric Wilcoxon signed-rank test (Wilcoxon, 1945) at the 5% significance level.

Table 1
Boundary conditions prescribed for the pre-industrial (PI) reference control and mid-Holocene (MH) climates.

	GHGs	Orbital forcing years B.P.	Saharan vegetation	Saharan dust
LI_{DS}	PI	0	desert	PI
HI_{DS}	MH	6000	desert	PI
HI_{GS}	MH	6000	shrubs	reduced

Table 2
List of the six climate indices used in this study out of the 27 from ETCCDI and their definitions.

Label	Definition of index	Unit
TXx	Annual maximum value of daily maximum temperature	°C
TNn	Annual minimum value of daily minimum temperature	°C
TRn	Annual number of nights with temperature ≤20 °C	Nights
CDD	Maximum number of consecutive days with RR < 1 mm	Days
RX5d	Annual maximum consecutive 5-day precipitation amount	mm
R1mm	Number of days with RR > 1 mm	Days

3. Results

In this section, we first present the annual and seasonal climatological changes in the temperature and precipitation distribution in the SSA domain during the high boreal summer insolation periods relative to the reference period of low boreal summer insolation (Subsection 3.1). We then investigate how climatological changes during high insolation periods are reflected in terms of changes in climate extremes over Zambia relative to low insolation periods (Subsection 3.2). Finally, we discuss changes in the seasonal cycle of temperature and precipitation at specific sites in Zambia (Subsection 3.3).

3.1. Changes in the annual and seasonal climatology of temperature

Zambia lies in the tropics, and its climate is characterized by two seasons: a dry season from May to October with a core ranging from June to August and a wet season from November to April, peaking from December to January. The annual mean temperature for the LI_{DS} simulation ranges from 16 to 22 °C in Zambia (Fig. 2a). More specifically, mean temperatures of 17.4 °C, 17.5 °C, and 21.4 °C were simulated in our three sub-regions (northeastern Zambia, Lusaka, and central Luangwa River Valley, respectively). The model has a cold bias in the region of approximately 2–2.5 °C. For instance, in Lusaka, the present-day observed annual mean temperature is 19.9 °C for the 1961–1990 period (National Oceanic and Atmospheric Administration – NOAA[1]), whereas the simulated pre-industrial temperature is approximately 17.5 °C. In the dry season, from May to October, the simulated seasonal mean temperature is slightly cooler in Lusaka (16.1 °C), followed by NE Zambia (16.5 °C) and Central Luangwa River Valley (20.4 °C) (Fig. 2d). The observed 1961–1990 dry season temperature is 18.3 °C in Lusaka (National Oceanic and Atmospheric Administration – NOAA[1]), which is 2.2 °C warmer than the simulated temperature for the region. As for the LI_{DS} humid season (November–April), simulated temperatures in the region range mainly between 18 °C and 24 °C (Fig. 2g). In the Central Luangwa River Valley, it is considerably warmer than in the two other locations because of its lower elevation as it reaches a seasonal mean of 22.3 °C compared to 18.4 °C in NE Zambia and 18.8 °C in Lusaka. The observed 1961–1990 humid season temperature is 2.7 °C warmer than the simulated temperature in Lusaka with an average of 21.5 °C (National Oceanic and Atmospheric Administration – NOAA[1]).

The mean annual temperature in the insolation alone (HI_{DS}) experiment compared to LI_{DS} generally shows a slight significant cooling over

[1] https://www.ncei.noaa.gov/access/monitoring/products/.

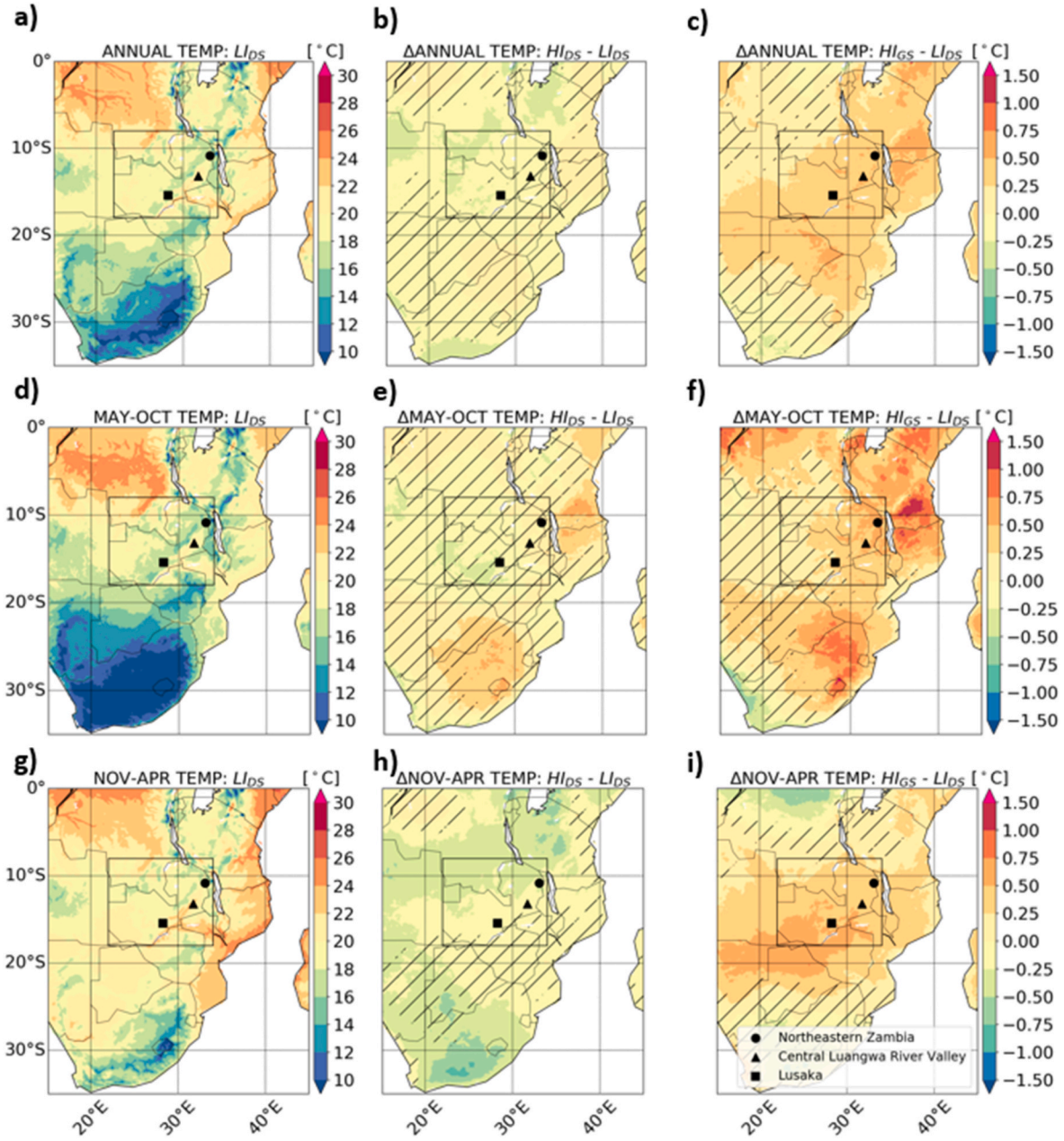

Fig. 2. Mean temperature for Low Insolation Dry Sahara (LI_{DS}) experiment (a–c) and anomalies for the High Insolation – Dry Sahara (HI_{DS}) (d–f) and the High Insolation – Green Sahara (HI_{GS}) (g–i) simulations for the annual (a, d, g), May–October (b, e, h) and November–April (c, f, i) climatology relative to LI_{DS}. Non-statistically significant anomalies at the 5% significance level are hatched.

Zambia, up to 0.5 °C in the north-western area (Fig. 2b). The only exception is represented by the region in the south-eastern part, where the mean annual temperature is not significantly affected by changes in insolation alone (Fig. 2b). During the dry season, the HI_{DS} exhibits small significant cold anomalies over southwest (SW) Zambia near Lusaka, up to approximately 0.25 °C, whereas temperatures in the northeast (NE) near the Central Luangwa River Valley region do not show any significant change (Fig. 2e). During the wet season, a slight but significant cooling is simulated in the HI_{DS} experiment compared to the LI_{DS} simulation over most of Zambia, peaking in the northern area with anomalies of up to 0.5 °C (Fig. 2h). The significant cooling also characterizes the region of the three selected areas with negative anomalies of approximately 0.25 °C.

The greening of the Sahara and dust reduction (Fig. 2c) show statistically significant warm anomalies between 0.25 °C and 0.50 °C for the entire Zambian subdomain relative to the LI_{DS} experiment. Over the central and eastern part of the subdomain the dry season temperature is higher than in the LI_{DS} experiment, by up to 0.6 °C in the NE part of Zambia (Fig. 2f), whereas the western part does not show a significant change compared to the LI_{DS} experiment Finally, in the wet season, significant positive anomalies occur in the region with up to 0.5 °C (Fig. 2i) in the HI_{GS} simulation relative to the LI_{DS} experiment.

In summary, slight cooling is simulated in all seasons for the HI_{DS} experiment relative to the LI_{DS}, being more pronounced in the wet season. Whereas significant warming during the entire year is shown in the HI_{GS} compared to the LI_{DS}.

3.2. *Changes in the annual and seasonal climatology of precipitation*

The annual mean rainfall in Zambia ranges between 2 and 6 mm/day

in the LI_{DS} simulation (Fig. 3a), with higher precipitation amounts in the northern section of the country. For example, the model simulates an annual rainfall of 3.1 mm/day for Lusaka, of about 3.7 mm/day for River Valley and of up to 4.2 mm/day for NE Zambia. The observed 1961–1990 precipitation in Lusaka is lower than that in the LI_{DS} simulation, amounting to approximately 2.4 mm/day (National Oceanic and Atmospheric Administration – NOAA[1]). During the dry season, from May to October, precipitation is very low with a simulated rainfall mean below 0.5 mm/day across the region (Fig. 3d), which compares well to the 1961–1990 Lusaka's observed precipitation reaching 0.13 mm/day (National Oceanic and Atmospheric Administration – NOAA[1]). During the wet season, i.e., from November to April (Fig. 4g), the main part of the annual precipitation occurs in Lusaka with an average of 5.9 mm/day of rainfall throughout that season, Central Luangwa River Valley averaged 6.9 mm/day and NE Zambia received 7.8 mm/day. The 1961–1990 observed precipitation for Lusaka is 4.7 mm/day (National Oceanic and Atmospheric Administration – NOAA[1]), which is 1.2 mm/day lower than the simulated precipitation.

Changes in the climatological mean precipitation over the study region do not show a clear signal in the HI_{DS} experiment relative to the LI_{DS}. In particular, the orbital forcing experiment alone (HI_{DS}) does not lead to statistically significant changes in annual precipitation for most of Zambia (Fig. 3b). As the dry months are characterized by scarce rainfall, no large change in precipitation is expected, with no significant changes in precipitation in the HI_{DS} experiment relative to the LI_{DS} during the dry season (Fig. 3e). During the wet season, an increase in precipitation in most locations of up to 0.6 mm/day is simulated in the HI_{DS} experiment relative to the LI_{DS} (Fig. 3h) in NE Zambia; however, the precipitation changes are generally statistically non-significant in all the locations.

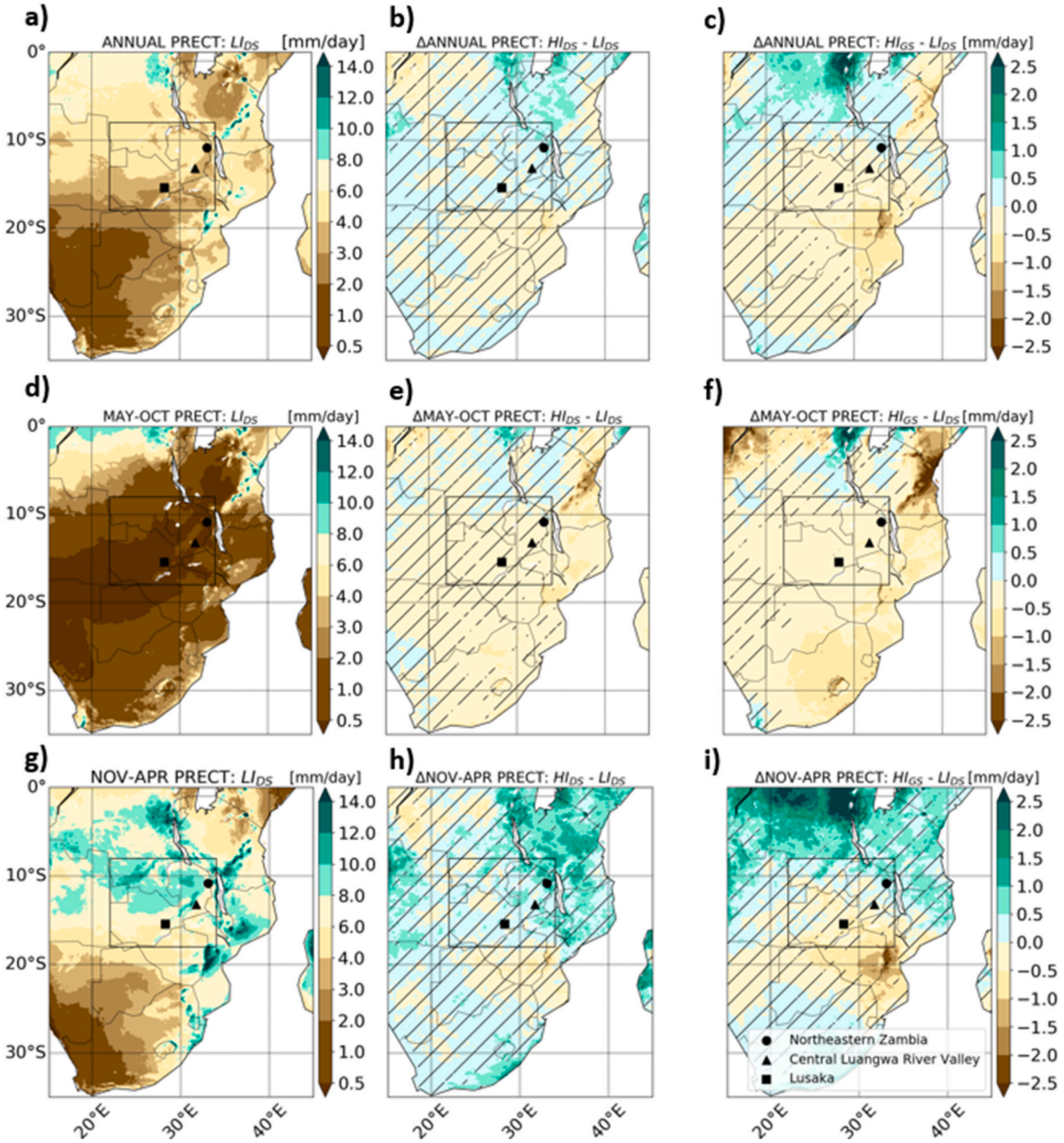

Fig. 3. Mean precipitation for Low Insolation - Dry Sahara (LI_{DS}) experiment (a–c) and anomalies in the High Insolation - Dry Sahara (HI_{DS}) (d–f) and in the High Insolation Green Sahara (HI_{GS}) (g–i) simulations for the annual (a, d, g), May–October (b, e, h) and November–April (c, f, i) climatology relative to LI_{DS}. Non-statistically significant anomalies at the 5% significance level are hatched.

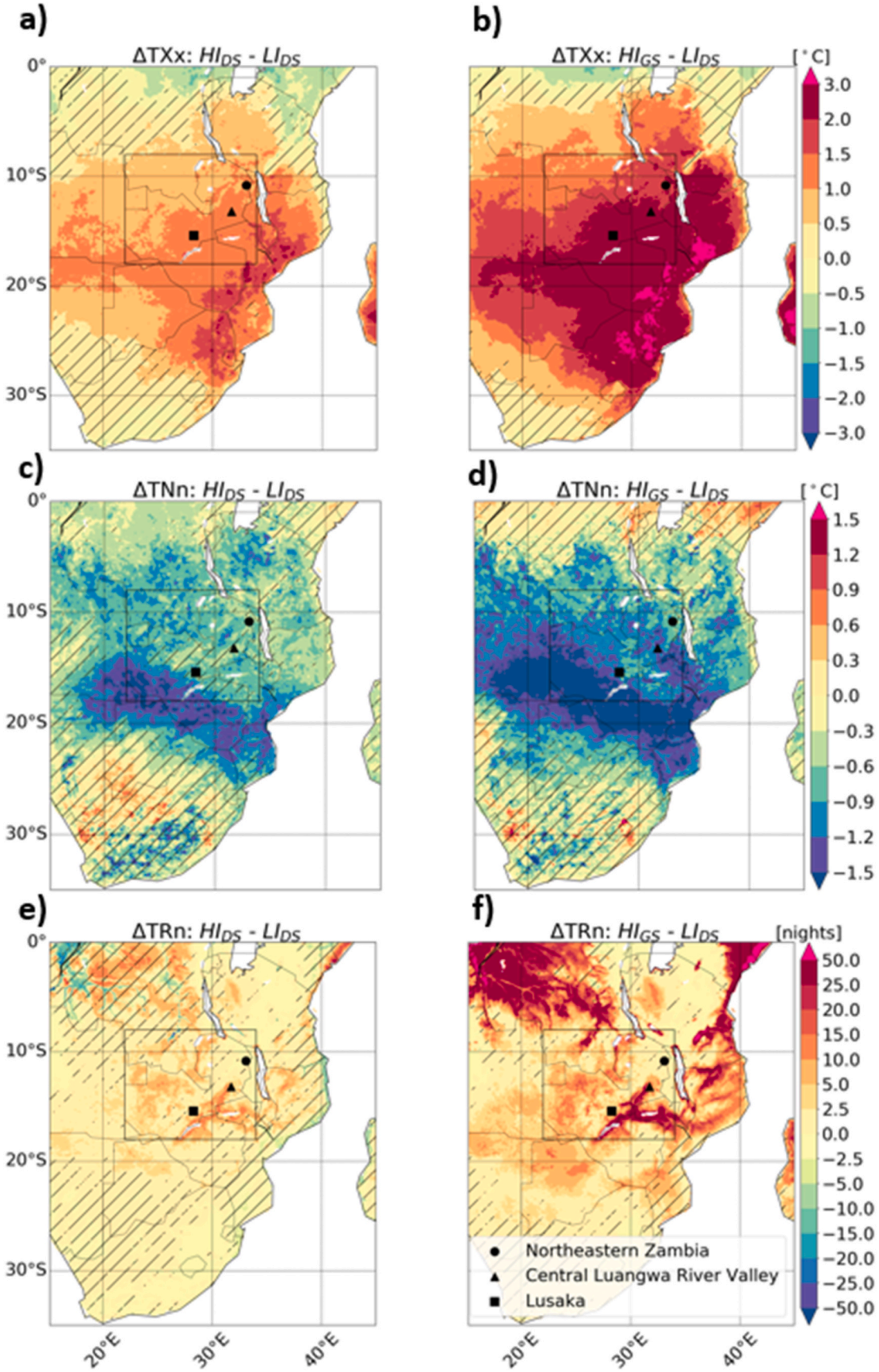

Fig. 4. Changes in the temperature of the annual hottest day (TXx, (a) and (b)), coldest night (TNn, (c) and (d)), and in the number of tropical nights (TRn (e) and (f)) for the HI_{DS} and HI_{GS} experiments relative to LI_{DS} simulation. Non-statistically significant anomalies at the 5% significance level are hatched.

The HI_{GS} experiment relative to the LI_{DS} shows a slight decrease in annual rainfall over the three study locations, being most pronounced in Lusaka (0.2 mm/day) (Fig. 3c). Moreover, a significant reduction in precipitation (up to 0.25 mm/day) is simulated in the HI_{GS} experiment across central southern Africa during the dry season (Fig. 3f). In the wet season, the Lusaka region sees significant reductions in precipitation of 0.25 mm/day in the HI_{GS} experiment relative to the LI_{DS} (Fig. 3i).

In summary, significant negative changes in precipitation are simulated in the HI_{GS} experiment over the whole Zambian subdomain in the dry season, and over the CAP (0.25 mm/day) in the wet season. The

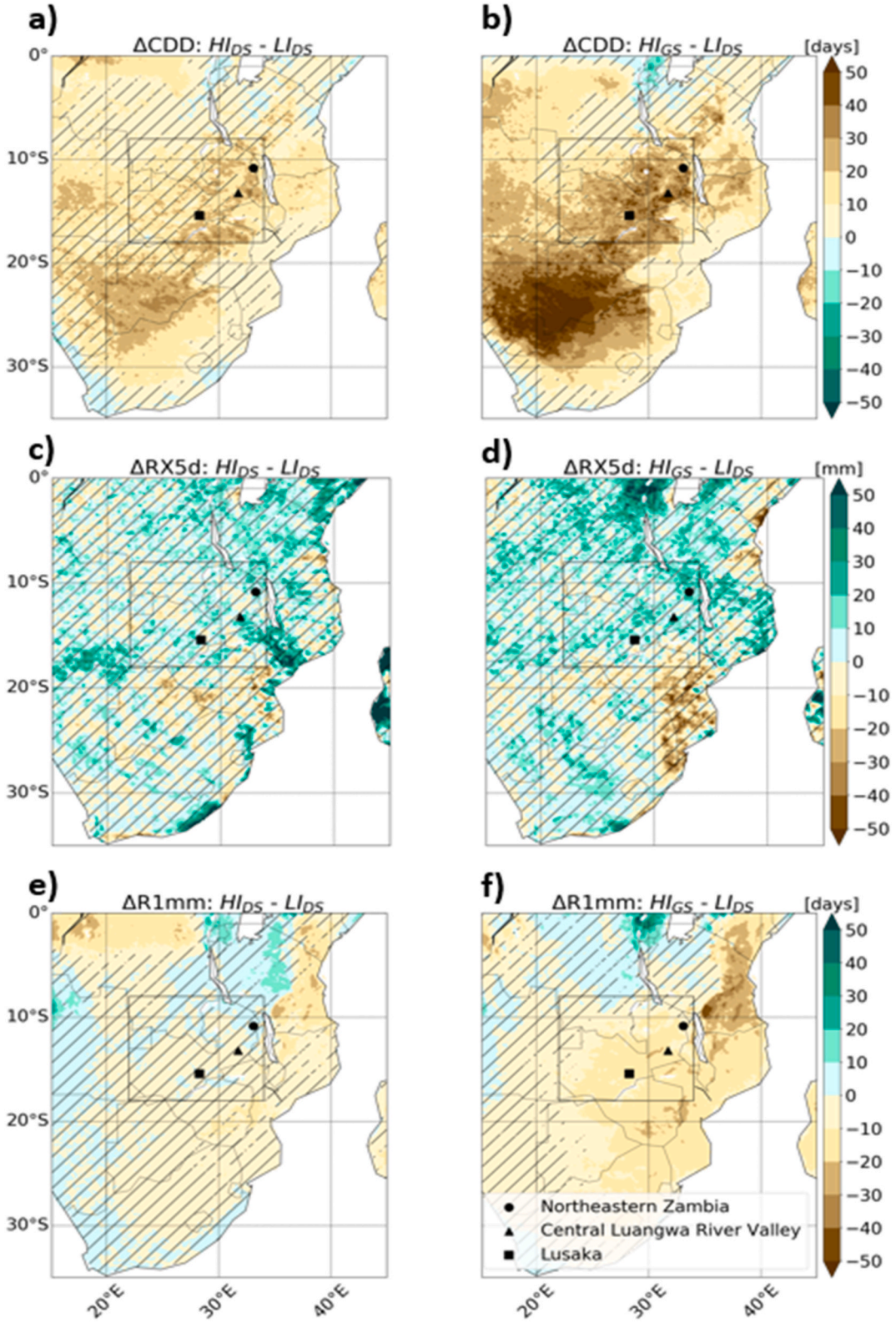

Fig. 5. Changes in the annual consecutive dry days (CDD, (a) and (b)), 5-day maximum precipitation (RX5day, (c) and (d)), and in the number of rainy days (R1mm (e) and (f)) for the HI_{DS} and HI_{GS} experiments relative to the LI_{DS} simulation. Non-statistically significant anomalies at the 5% significance level are hatched.

overall annual precipitation slightly decreases in Lusaka (0.2 mm/day) in the HI_{GS} experiment relative to the LI_{DS}, although the changes are not significant. The HI_{DS} experiment does not show any significant annual and seasonal change relative to LI_{DS}.

3.3. Changes in climate extremes: indices of temperature

Changes in solar insolation alone (HI_{DS}) lead to a temperature increase for the hottest day of the year (TXx) of up to 1.2 °C relative to the LI_{DS} experiment, throughout Zambia, and especially in the southern part (Fig. 4a). In contrast, the lowest temperature of the year (TNn) is lower in the HI_{DS} experiment (Fig. 4c). Relative to the $LI_{DS,}$ it exhibits a decrease of up to 0.5 °C in TNn in the NE part of Zambia, a more notable decrease of 0.7 °C is simulated in the Lusaka and Central Luangwa River Valley region and a decrease of up to 1.5 °C in the southwestern part of the country, including the CAP (1 °C). An increase in the number of tropical nights (TRn) of about five nights is simulated for the HI_{DS} experiment for the River Valley relative to the LI_{DS} simulation. On the other hand, no statistically significant TRn change was detected for NE Zambia and Lusaka (Fig. 4e).

When considering the changes in Saharan vegetation and dust concentration (HI_{GS}), the pattern in TXx changes is similar to the HI_{DS} pattern, however, the positive anomalies are amplified with values of up to 3 °C in the SE part of the country, including Central Luangwa River Valley and Lusaka locations. Over the CAP, the temperature anomalies are slightly less pronounced (~2 °C) (Fig. 4b). The pattern in TNn changes for the HI_{GS} experiment is comparable to that of the HI_{DS}, although the negative anomalies are amplified: 1.5 °C over the CAP and nearly 1 °C in the Central Luangwa River Valley (Fig. 4d). The River Valley has seen a significant increase of 14 TRn in the HI_{GS} experiment relative to the LI_{DS}, while no statistically significant TRn change was simulated for the two other locations (Fig. 4f).

Overall, our results show that Sahara greening plays an important role in affecting temperature extremes, leading to more extreme temperatures in southern tropical Africa for both the low and high values relative to HI_{DS} and LI_{DS} simulations with major differences between the Central Luangwa River Valley and the CAP.

3.4. Changes in climate extremes indices of precipitation

The orbital forcing alone (HI_{DS}) causes an increase in the drought duration over the entire Zambia subdomain (Fig. 5a) as shown by the changes in consecutive dry days (CDD) annual means. This increase is generally not significant, except for the SE area. The CAP region, including Lusaka, presents the higher CDD anomalies with an increase of 23 days (22%), followed by the NE part of Zambia with 22 days (34%), and finally the Central Luangwa River Valley region with an increase in CCD of 12 days (16%). The 5-day maximum precipitation amount (RX5day) also intensified as rainfall increases, ranging from 7 mm in Lusaka (7%) and the Central Luangwa River Valley (5%) to nearly 13 mm in NE Zambia (8%) (Fig. 5c) although this change is generally not significant over the all Zambia. No significant change in the total number of rainy days (R1mm) is simulated under insolation forcing alone (Fig. 5e).

Saharan vegetation and reduction in dust concentrations (HI_{GS}) increase the CDD over all of Zambia, amplifying the anomalies simulated in the HI_{DS} experiment, particularly in the southern and western parts of the country (Fig. 5b). An increase of 27 CDD is simulated in the Central Luangwa River Valley, more than doubling compared to the HI_{DS}, and the lowest increase is now found in NE Zambia with 25 CDD relative to the LI_{DS}. The longest duration of dry spells is simulated in Lusaka, with an increase of over a month (39 days) in CDD relative to the LI_{DS} experiment. The RX5d index presents similar, albeit weaker, results for the HI_{GS} simulation as for the HI_{DS} (Fig. 5d), with all changes being not statistically significant. In the HI_{GS} experiment, the number of rainy days (R1mm) is significantly decreased by up to 12 days in Lusaka, followed by NE Zambia and Central Luangwa River Valley with a decrease of 11 and 9 days respectively relative to the LI_{DS} (Fig. 5f).

In summary, the combined impact of increased boreal summer insolation and Sahara greening caused drying in the study region during all seasons. Drought duration is enhanced in the HI_{GS}, as shown by the number of consecutive dry days, especially over the CAP (39 days), followed by the Central Luangwa River Valley (27 days), compared to the LI_{DS} experiment. A significant decrease in rainy days is shown by HI_{GS} relative to LI_{DS} during the wet season over the whole region where the selected areas lie.

3.5. Regional changes in seasonal cycles of mean temperature and precipitation

In this section, we present the temperature and precipitation seasonal cycle of all three experiments; for simplicity, we only show NE Zambia; however, the results are similar for all of Zambia. The temperature peaks in the pre-monsoonal season with the warmest month in October, while the coldest season is from May to July with the coldest month in June. The rainfall seasonality is characterized by a dry season with no or little rainfall from May to October and a rainy season from November to April.

The seasonal temperature cycle shows a temperature increase at the end of the dry season, from September to November, in the HI_{DS} simulation relative to the LI_{DS} (Fig. 6a). The temperature increase is nearly 0.5 °C in September and November, with a significant peak of approximately 1.5 °C in October. Throughout the remainder of the year, no significant temperature changes were simulated in the HI_{DS} experiment.

Saharan vegetation change and dust reduction during a Green Sahara state (HI_{GS}) present similar results. However, the temperature change is amplified from September to November, with higher significant values of nearly 1.5 °C and 2 °C in September and November, respectively, and a peak in October of about 2.5 °C relative to the LI_{DS}. As in the HI_{DS}, the HI_{GS} shows no statistically significant temperature change throughout the rest of the year relative to the LI_{DS}.

In the HI simulations, the climatological seasonal precipitation cycle exhibits an increase during the core of the humid season in December and January, relative to the LI_{DS} (Fig. 6b). Rainfall increases by up to 2.5 and 3 mm/day for HI_{DS} and HI_{GS} in December and January, respectively. A small reduction of nearly 0.5 mm/day is simulated for both HI simulations relative to the LI_{DS} at the start of the humid season in October and November and at the start of the dry season in March and April. Throughout the rest of the year, from May to September, no statistically significant precipitation change is simulated.

In conclusion, our simulations show a shift forward in the rainfall associated with the summer monsoon and enhanced aridity in the dry season. The decrease in precipitation in the dry season in the HI simulations relative to the LI experiment is associated with an increase in the divergence aloft **and subsidence at the surface** that intensifies in the HI_{GS} relative to HI_{DS} (Fig. 7). Such an increase in the divergence aloft enhances arid conditions during the dry season over Zambia (Fig. 3e and f, and 5a and b). The average monthly temperature increases in the pre-monsoonal season (August through November) in the HI_{GS} relative to the LI_{DS}. The fall and early winter temperature (February to June) are instead below average. Such anomalous behavior is identical in the HI_{DS} and HI_{GS} experiments, as it is mostly driven by the changes in solar insolation with an increase in late winter and spring insolation (August to November) and a decrease during summer and fall (December to May). However, the temperature anomalies in the HI_{GS} are larger than in the HI_{DS} in austral winter due to warmer advections as the temperature in the central and eastern equatorial Africa are remarkably higher (compare panels e and f in Fig. 2). The more pronounced anomalies simulated in the HI_{GS} relative to the HI_{DS} experiments highlight the far-reaching role of vegetation.

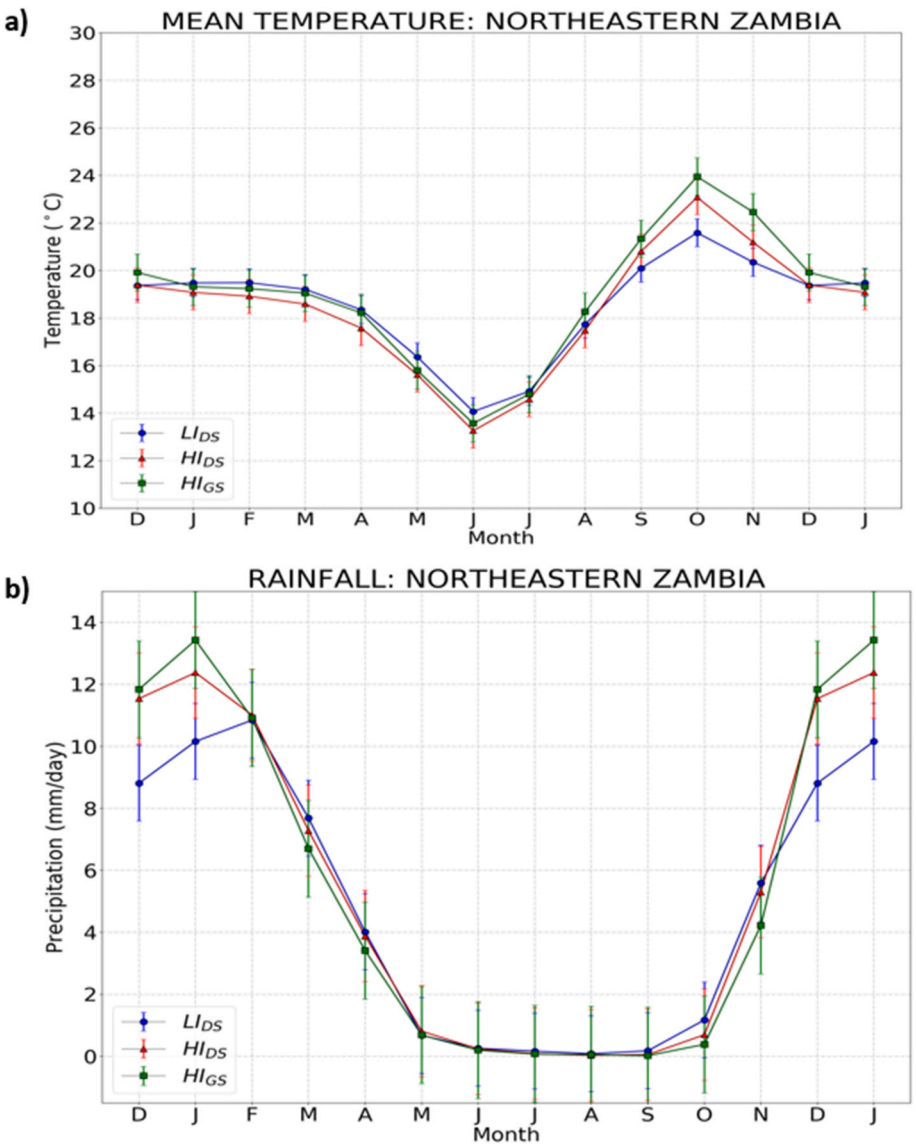

Fig. 6. a) Temperature and **b)** precipitation climatological seasonal cycle in northeastern Zambia for LI_{DS} (blue), HI_{DS} (red), and HI_{GS} (green) simulations. Error bars indicate standard errors of the means.

4. Discussion and conclusions

In this study, we show that vegetation changes over the Sahara and the associated reduction in airborne dust concentrations during periods of high boreal summer insolation (HI_{GS}) remarkably impact temperature and rainfall in SSA and Zambia, in particular. During the HI_{DS}, the changes in annual and seasonal temperature in Zambia are small, being only slightly warmer than in the LI_{DS}. From September to November, temperature and precipitation extremes change significantly under HI_{GS} conditions relative to the low insolation and dry Sahara (LI_{DS}) case. In particular, the hottest day (TXx) and the coldest night of the year (TNx) become more extreme with an increase of up to 3 °C and a decrease of up to 1.5 °C, respectively. The number of rainy days (R1mm) decreases by approximately 10 days in Lusaka relative to the LI_{DS} experiment, which has a total of 102 rainy days per year. This means that, in the HI_{GS} experiment, there is a 10% reduction in the number of rainy days per year. Droughts also become more extended under HI_{GS} conditions relative to the LI_{DS} conditions, with an increase in CDDs of over a month in the southern part of Zambia. Overall, the model simulates hotter AHP conditions in southern tropical Africa. The results also show a major difference in rainfall changes and the length of droughts between the CAP and the Central Luangwa River Valley. These results highlight the potentially crucial role played by the Zambezi drainage and the Luangwa River Valley as key water resources for seasonal hominin mobility, especially during the dry season.

The simulated changes in temperature and precipitation over Zambia are largely a result of changes in solar insolation and the modification in the atmospheric dynamics induced by the strengthening of the West African Monsoon. In general, the anomaly pattern seen in the HI_{GS} experiment relative to the LI_{DS} is very similar to the HI_{DS}, but it is more intense, highlighting the central role of the West African Monsoon in altering atmospheric circulation over Africa and hence affecting southern tropical Africa. In Zambia, the impact of these changes is also influenced by local topography, with distinctly drier and more drought-prone conditions in the Central Plateau relative to the Zambezi drainage during the HI_{GS} relative to the LI_{DS}. The insolation changes during the mid-Holocene (i.e., higher insolation from June to November and lower from December to May) are responsible for the higher temperature extremes (Fig. 4a and b) as well as a higher number of tropical nights (Fig. 4e and f). Temperature extremes in Zambia are recorded in the pre-monsoonal dry season, i.e., from September to November, which coincide with the increase in insolation in the region. The decrease in

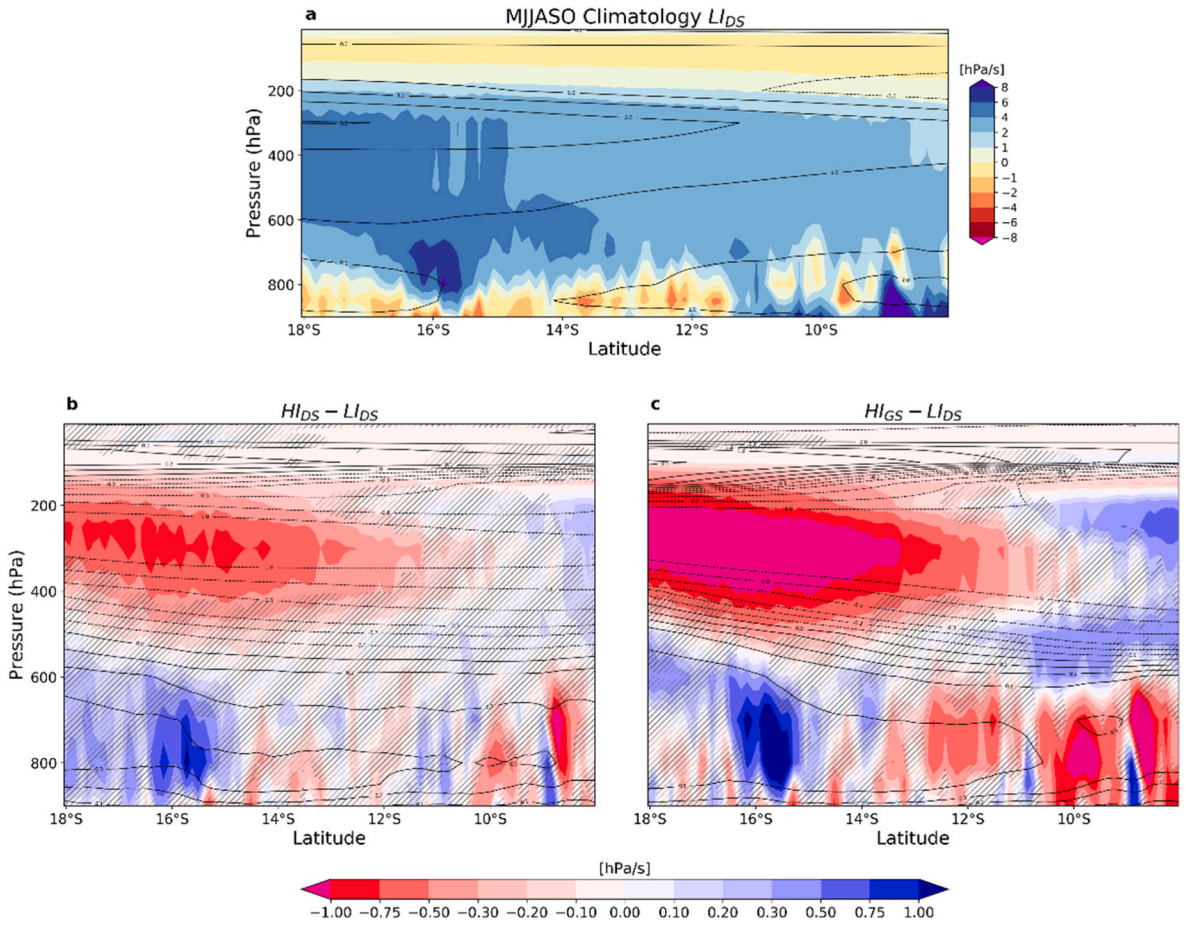

Fig. 7. Meridional and vertical circulation. a) Climatological meridional circulation (contours, m/s) and vertical motion (shaded) averaged between 22°E and 35°E for the period May–October (MJJASO) and their changes for b) HI_{DS} and c) HI_{GS} relatively to pre-industrial (L_{IDS}). Positive (blue) values of vertical motion indicate downward motion while positive values of meridional circulation indicate northward direction. Hatched areas cover the areas where the changes are not statistically significant at 5% of significance level.

insolation during the boreal summer and fall (January to May) is causing lower monthly mean temperatures until the beginning of winter (Fig. 6a), explaining the drop in low temperature extremes (Fig. 4c and d). Therefore, changes in temperature extremes, despite no changes or slight cooling in the annual mean, are essentially due to increased insolation between July and November and decreased insolation between December and May.

Although we use the middle Holocene and pre-industrial boundary conditions and orbital forcing, our simulations can be seen as an archetypal of other high and low boreal summer insolation forcing. However, MH orbital forcing were far from being extreme: for example, summer insolation was much stronger during the Eemian (128,000–122,000 years ago) or even during the early Holocene (11,000–8000 years ago; Otto-Bliesner et al., 2016).

The extreme conditions seen in our HI_{GS} scenario, may have altered patterns of hominin mobility, thus affecting the course of hominin evolution in Africa and were likely even more extreme during other HI periods, when insolation changes were even larger than those simulated in our experiments. According to our simulations, the CAP experienced less rainfall during the dry season, from May to October, under AHP conditions with an increase in the number of consecutive dry days and more arid conditions. On a regional scale, the savanna landscapes of the CAP would consequently have changed, becoming less favorable for human habitation, especially during the extended dry season. As the CAP became less hospitable, the resources offered by large river drainages such as the Zambezi and its tributaries, such as the Luangwa River, would have been critical to hominin survival, guiding their seasonal mobility (Barham, 2000; Burrough et al., 2019). The fluctuation between more aridity during the AHPs and less aridity during the dry Sahara in the Luangwa Valley also has implications for the inferred depositional history of the region and thus, the regional archaeological record (Burke et al., 2023; Colton et al., 2021). More arid conditions in the CAP, which would have seasonally constrained human mobility, occurred at a time when hydrological systems in the Sahel and the Sahara were activated, opening "green corridors" that would have facilitated genetic and cultural exchange on a continental scale, once again highlighting the importance of Central African river systems. Given the recurrence of the AHPs, our results would imply a cyclicity in the pattern and the timing of population migration across northern and central Africa with serious implications for the pattern of hominin evolution, as has recently been suggested (Hublin et al., 2017).

In conclusion, the results of this study show that AHPs affect Southern Tropical Africa, making it a more arid environment overall - possibly constraining hominin mobility at a time when movement across the Sahara Desert would have been possible. This could have enhanced the role of large river systems such as the Luangwa River, which would have acted as refugia and biogeographic corridors (Barham, 2000; Barham et al., 2011). Perhaps not coincidentally, hominin occupations of the Luangwa valley occurred under more arid conditions (Colton et al., 2021). Continuing archaeological research in the Luangwa Basin may help resolve whether climatic fluctuations drove patterns of human occupation and movement in the area during prehistory (Burke et al., 2023).

Declaration of competing interest

The authors declare that they have no known competing financial interests or personal relationships that could have appeared to influence the work reported in this paper.

Data availability

Data will be made available on request.

Acknowledgments

The authors would like to thank the Recherche en Prévision Numérique (RPN), the Meteorological Research Branch (MRB) and the Canadian Meteorological Centre (CMC) for the permission to use the GEM model as basis for our CRCM5 regional climate model; and Qiong Zhang for sharing the global model outputs. This research was enabled in part by support provided by Calcul Quebec (https://www.calculquebec.ca/, last access: July 1, 2023) and the Digital Research Alliance of Canada (https://alliancecan.ca/en last access: July 1, 2023). F.S.R.P, D.A. and R.I. acknowledge the financial support from the Natural Sciences and Engineering Research Council of Canada (NSERC; Grant RGPIN-2018-04981). F.S.R.P., D.A., A.B. and M.D. also acknowledges the financial support from the Fond de recherche du Québec Société et Culture (FRQSC; Grant 2019-SE3-254686).

References

Abbate, E., Sagri, M., 2012. Early to middle Pleistocene Homo dispersals from Africa to eurasia: geological, climatic and environmental constraints. Quat. Int. 267, 3–19. https://doi.org/10.1016/J.QUAINT.2011.02.043.

Agustí, J., Lordkipanidze, D., 2011. How "African" was the early human dispersal out of Africa? Quat. Sci. Rev. 30 (11–12), 1338–1342. https://doi.org/10.1016/J.QUASCIREV.2010.04.012.

Armstrong, E., Tallavaara, M., Hopcroft, P.O., Valdes, P.J., 2023. North African humid periods over the past 800,000 years. Nat. Commun. 14 (1), 1–11. https://doi.org/10.1038/s41467-023-41219-4, 2023 14:1.

Barham, Larry, 2000. The Middle Stone Age of Zambia, South Central Africa. Western academic & specialist Press. Retrieved from. https://www.amazon.com.br/Middle-Stone-Zambia-Central-Africa/dp/095354186X.

Barham, Lawrence, Phillips, W.M., Maher, B.A., Karloukovski, V., Duller, G.A.T., Jain, M., Wintle, A.G., 2011. The dating and interpretation of a Mode 1 site in the Luangwa Valley, Zambia. J. Hum. Evol. 60 (5), 549–570. https://doi.org/10.1016/J.JHEVOL.2010.12.003.

Benoit, R., Côté, J., Mailhot, J., 1989. Inclusion of a TKE boundary layer parameterization in the Canadian regional finite-element model. Mon. Weather Rev. 117 (8), 1726–1750. https://doi.org/10.1175/1520-0493(1989)117.

Berger, A., 1978. Long-term variations of daily insolation and quaternary climatic changes. J. Atmos. Sci. 35 (12), 2362–2367. https://doi.org/10.1175/1520-0469(1978)035<2362:LTVODI>2.0.CO;2.

Blome, M.W., Cohen, A.S., Tryon, C.A., Brooks, A.S., Russell, J., 2012. The environmental context for the origins of modern human diversity: a synthesis of regional variability in African climate 150,000–30,000 years ago. J. Hum. Evol. 62 (5), 563–592. https://doi.org/10.1016/J.JHEVOL.2012.01.011.

Burke, A., Bisson, M., Schilt, F., Tolan, S., Museba, J., Drapeau, M.S.M., et al., 2023. The archaeological potential of the northern Luangwa Valley, Zambia: the Luwumbu basin. PLoS One 18 (3), e0269209. https://doi.org/10.1371/JOURNAL.PONE.0269209.

Burke, Ariane, Peros, M.C., Wren, C.D., Pausata, F.S.R., Riel-Salvatore, J., Moine, O., et al., 2021. The archaeology of climate change: the case for cultural diversity. Proc. Natl. Acad. Sci. U.S.A. 118 (30) https://doi.org/10.1073/pnas.2108537118.

Burrough, S.L., Thomas, D.S.G., Barham, L.S., 2019. Implications of a new chronology for the interpretation of the middle and later Stone age of the upper Zambezi valley. J. Archaeol. Sci.: Reports 23, 376–389. https://doi.org/10.1016/J.JASREP.2018.10.016.

Castañeda, I.S., Mulitza, S., Schefuss, E., Lopes dos Santos, R.A., Sinninghe Damsté, J.S., Schouten, S., 2009. Wet phases in the Sahara/Sahel region and human migration patterns in North Africa. Proc. Natl. Acad. Sci. U.S.A. 106 (48), 20159–20163. https://doi.org/10.1073/pnas.0905771106.

Colton, D., Whitfield, E., Plater, A.J., Duller, G.A.T., Jain, M., Barham, L., 2021. New geomorphological and archaeological evidence for drainage evolution in the Luangwa Valley (Zambia) during the Late Pleistocene. Geomorphology 392, 107923. https://doi.org/10.1016/J.GEOMORPH.2021.107923.

Daly, M.C., Green, P., Watts, A.B., Davies, O., Chibesakunda, F., Walker, R., 2020. Tectonics and landscape of the central African Plateau and their implications for a propagating southwestern Rift in Africa. G-cubed 21 (6), e2019GC008746. https://doi.org/10.1029/2019GC008746.

Dandoy, S., Pausata, F.S.R., Camargo, S.J., Laprise, R., Winger, K., Emanuel, K., 2021. Atlantic hurricane response to Saharan greening and reduced dust emissions during the mid-Holocene. Clim. Past 17 (2), 675–701. https://doi.org/10.5194/CP-17-675-2021.

Delage, Y., 1997. Parameterising sub-grid scale vertical transport in atmospheric models under statically stable conditions. Boundary-Layer Meteorol. 82 (1), 23–48. https://doi.org/10.1023/A:1000132524077.

Delage, Y., Girard, C., 1992. Stability functions correct at the free convection limit and consistent for for both the surface and Ekman layers. Boundary-Layer Meteorol. 58 (1–2), 19–31. https://doi.org/10.1007/BF00120749/METRICS.

deMenocal, P., Ortiz, J., Guilderson, T., Adkins, J., Sarnthein, M., Baker, L., Yarusinsky, M., 2000. Abrupt onset and termination of the african humid period. Quat. Sci. Rev. 19 (1–5), 347–361. https://doi.org/10.1016/S0277-3791(99)00081-5.

deMenocal, P.B., Tierney, J.E., 2012. Green Sahara: african humid periods paced by Earth's orbital changes. Nature Education Knowledge 3 (10).

Drake, N.A., Blench, R.M., Armitage, S.J., Bristow, C.S., White, K.H., 2011. Ancient watercourses and biogeography of the Sahara explain the peopling of the desert. Proc. Natl. Acad. Sci. U.S.A. 108 (2), 458–462. https://doi.org/10.1073/pnas.1012231108.

Fauchereau, N., Trzaska, S., Rouault, M., Richard, Y., 2003. Rainfall variability and changes in Southern Africa during the 20th century in the global warming context. Nat. Hazards 29 (2), 139–154. https://doi.org/10.1023/A:1023630924100/METRICS.

Gaetani, M., Messori, G., Zhang, Q., Flamant, C., Pausata, F.S.R., 2017. Understanding the mechanisms behind the northward extension of the West African Monsoon during the mid-Holocene. J. Clim. 30 (19) https://doi.org/10.1175/JCLI-D-16-0299.1.

Gasse, F., 2000. Hydrological changes in the african tropics since the last glacial maximum. Quat. Sci. Rev. 19 (1–5), 189–211. https://doi.org/10.1016/S0277-3791(99)00061-X.

Gasse, F., Téhet, R., Durand, A., Gibert, E., Fontes, J.C., 1990. The arid–humid transition in the Sahara and the Sahel during the last deglaciation. Nature 346 (6280), 141–146. https://doi.org/10.1038/346141a0, 1990 346:6280.

Girard, C., Plante, A., Desgagné, M., Mctaggart-Cowan, R., Côté, J., Charron, M., et al., 2014. Staggered vertical discretization of the Canadian environmental Multiscale (GEM) model using a coordinate of the log-hydrostatic-pressure type. Mon. Weather Rev. 142 (3), 1183–1196. https://doi.org/10.1175/MWR-D-13-00255.1.

Hély, C., Lézine, A.-M., contributors, A., 2014. Holocene changes in African vegetation: tradeoff between climate and water availability. Clim. Past 10 (2), 681–686. https://doi.org/10.5194/cp-10-681-2014.

Hoelzmann, P., Jolly, D., Harrison, S.P., Laarif, F., Bonnefille, R., Pachur, H.-J., 1998. Mid-Holocene land-surface conditions in northern Africa and the Arabian Peninsula: a data set for the analysis of biogeophysical feedbacks in the climate system. Global Biogeochem. Cycles 12 (1), 35–51. https://doi.org/10.1029/97GB02733.

Hublin, J.J., Ben-Ncer, A., Bailey, S.E., Freidline, S.E., Neubauer, S., Skinner, M.M., et al., 2017. New fossils from Jebel Irhoud, Morocco and the pan-African origin of Homo sapiens. Nature 546 (7657), 289–292. https://doi.org/10.1038/nature22336, 2017 546:7657.

Kain, J.S., Fritsch, J.M., 1990. A one-dimensional entraining/detraining plume model and its application in convective parameterization. J. Atmos. Sci. 47 (23), 2784–2802. https://doi.org/10.1175/1520-0469(1990)047.

Klein, R.G., Richard Klein, C.G., 2019. Population structure and the evolution of Homo sapiens in Africa. Evol. Anthropol. Issues News Rev. 28 (4), 179–188. https://doi.org/10.1002/EVAN.21788.

Kuo, H.L., 1965. On Formation and intensification of tropical cyclones through latent heat release by cumulus convection. J. Atmos. Sci. 22 (1), 40–63. https://doi.org/10.1175/1520-0469(1965)022.

Kutzbach, J.E., 1981. Monsoon climate of the early Holocene: climate experiment with the Earth's orbital parameters for 9000 Years ago. Science (New York, N.Y.) 214 (4516), 59–61. https://doi.org/10.1126/science.214.4516.59.

Kutzbach, John E., Guan, J., He, F., Cohen, A.S., Orland, I.J., Chen, G., 2020. African climate response to orbital and glacial forcing in 140,000-y simulation with implications for early modern human environments. Proc. Natl. Acad. Sci. U.S.A. 117 (5), 2255–2264. https://doi.org/10.1073/PNAS.1917673117/SUPPL_FILE/PNAS.1917673117.SAPP.PDF.

Larrasoaña, J.C., Roberts, A.P., Rohling, E.J., 2013. Dynamics of green Sahara periods and their role in hominin evolution. PLoS One 8 (10), e76514. https://doi.org/10.1371/journal.pone.0076514.

Li, J., Barker, H.W., 2005. A radiation algorithm with correlated-k distribution. Part I: local thermal equilibrium. J. Atmos. Sci. 62 (2), 286–309. https://doi.org/10.1175/JAS-3396.1.

Manhique, A.J., Reason, C.J.C., Silinto, B., Zucula, J., Raiva, I., Congolo, F., Mavume, A. F., 2015. Extreme rainfall and floods in southern Africa in January 2013 and associated circulation patterns. Nat. Hazards 77 (2), 679–691. https://doi.org/10.1007/S11069-015-1616-Y/FIGURES/9.

Martynov, A., Sushama, L., Laprise, R., Winger, K., Dugas, B., 2012. Interactive lakes in the Canadian Regional Climate Model, version 5: the role of lakes in the regional climate of North America. New Pub: Stockholm Uni Press 64 (1). https://doi.org/10.3402/TELLUSA.V64I0.16226.

Mason, S.J., Jury, M.R., 1997. Climatic variability and change over southern Africa: a reflection on underlying processes 21 (1), 23–50. https://doi.org/10.1177/030913339702100103. Http://Dx.Doi.Org/10.1177/030913339702100103.

Masson, V., Champeaux, J.-L., Chauvin, F., Meriguet, C., Lacaze, R., Masson, V., et al., 2003. A global database of land surface parameters at 1-km resolution in

meteorological and climate models. J. Clim. 16 (9), 1261–1282. https://doi.org/10.1175/1520-0442-16.9.1261.
McFarlane, & A., N., 1987. The effect of orographically excited gravity wave drag on the general circulation of the lower stratosphere and troposphere. J. Atmos. Sci. 44 (14), 1775–1800. https://doi.org/10.1175/1520-0469(1987)044.
McTaggart-Cowan, R., Vaillancourt, P.A., Zadra, A., Chamberland, S., Charron, M., Corvec, S., et al., 2019. Modernization of atmospheric physics parameterization in Canadian NWP. J. Adv. Model. Earth Syst. 11 (11), 3593–3635. https://doi.org/10.1029/2019MS001781.
Nicholson, S.E., 2019. A review of climate dynamics and climate variability in eastern Africa. The Limnology, Climatology and Paleoclimatology of the East African Lakes 25–56. https://doi.org/10.1201/9780203748978-2.
Osborne, A.H., Vance, D., Rohling, E.J., Barton, N., Rogerson, M., Fello, N., 2008. A humid corridor across the Sahara for the migration of early modern humans out of Africa 120,000 years ago. Proc. Natl. Acad. Sci. U.S.A. 105 (43), 16444–16447. https://doi.org/10.1073/pnas.0804472105.
Otto-Bliesner, B.L., Braconnot, P., Harrison, S.P., Lunt, D.J., Abe-Ouchi, A., Albani, S., et al., 2016. The PMIP4 contribution to CMIP6. Part 2: two interglacials, scientific objective and experimental design for Holocene and last interglacial simulations. Geosci. Model Dev. (GMD) 10, 3979–4003. https://doi.org/10.5194/gmd-2016-279.
Pausata, F.S.R., Zhang, Q., Muschitiello, F., Lu, Z., Chafik, L., Niedermeyer, E.M., et al., 2017a. Greening of the Sahara suppressed ENSO activity during the mid-Holocene. Nat. Commun. 8 https://doi.org/10.1038/ncomms16020.
Pausata, F.S.R., Emanuel, K.A., Chiacchio, M., Diro, G.T., Zhang, Q., Sushama, L., et al., 2017b. Tropical cyclone activity enhanced by Sahara greening and reduced dust emissions during the African Humid Period. Proc. Natl. Acad. Sci. U.S.A. 114 (24), 6221–6226. https://doi.org/10.1073/pnas.1619111114.
Pausata, F.S.R., Messori, G., Yun, J., Jalihal, C.A., Bollasina, M.A., Marchitto, T.M., 2021. The remote response of the South Asian Monsoon to reduced dust emissions and Sahara greening during the middle Holocene. Clim. Past 17 (3), 1243–1271. https://doi.org/10.5194/CP-17-1243-2021.
Pausata, Francesco S.R., Messori, G., Zhang, Q., 2016. Impacts of dust reduction on the northward expansion of the African monsoon during the Green Sahara period. Earth Planet Sci. Lett. 434, 298–307. https://doi.org/10.1016/j.epsl.2015.11.049.
Piao, J., Chen, W., Wang, L., Pausata, F.S.R., Zhang, Q., 2020. Northward extension of the East Asian summer monsoon during the mid-Holocene. Global Planet. Change 184, 103046. https://doi.org/10.1016/J.GLOPLACHA.2019.103046.
Reynolds, S.C., 2015. The role of landscapes in shaping hominin habitats in Africa. In: Sankhyan, A.R. (Ed.), Recent Discoveries and Perspectives in Human Evolution. British Archaeological Reports, Oxford, England, pp. 68–76. Retrieved from. https://staffprofiles.bournemouth.ac.uk/display/chapter/210794.
Richard, Y., Fauchereau, N., Poccard, I., Rouault, M., Trzaska, S., 2001. 20th century droughts in southern Africa: spatial and temporal variability, teleconnections with oceanic and atmospheric conditions. Int. J. Climatol. 21 (7), 873–885. https://doi.org/10.1002/JOC.656.
Richter, D., Grün, R., Joannes-Boyau, R., Steele, T.E., Amani, F., Rué, M., et al., 2017. The age of the hominin fossils from jebel irhoud, Morocco, and the origins of the middle Stone Age. Nature 546 (7657), 293–296. https://doi.org/10.1038/nature22335.
Scerri, E.M.L., 2017. The North african middle Stone age and its place in recent human evolution. Evol. Anthropol. Issues News Rev. 26 (3), 119–135. https://doi.org/10.1002/EVAN.21527.
Smith, J.R., 2012. Spatial and temporal variation in the nature of Pleistocene pluvial phase environments across north Africa. Vertebrate Paleobiology and Paleoanthropology (9789400729285), 35–47. https://doi.org/10.1007/978-94-007-2929-2_3/COVER.
Stringer, C., Galway-Witham, J., 2017. On the origin of our species. Nature 546 (7657), 212–214. https://doi.org/10.1038/546212a, 2017 546:7657.
Sun, W., Wang, B., Zhang, Q., Pausata, F.S.R., Chen, D., Lu, G., et al., 2019. Northern Hemisphere land monsoon precipitation increased by the green Sahara during middle Holocene. Geophys. Res. Lett. 46 (16), 9870–9879. https://doi.org/10.1029/2019GL082116.
Sundquist, H., Berge, E., Kristjansson, J.E., 1989. Condensation and cloud parameterization studies with a mesoscale numerical prediction model. Mon.Wea. Rev. 117, 1641–1657.
Szabo, B.J., Haynes, C.V., Maxwell, T.A., 1995. Ages of Quaternary pluvial episodes determined by uranium-series and radiocarbon dating of lacustrine deposits of Eastern Sahara. Palaeogeogr. Palaeoclimatol. Palaeoecol. 113 (2–4), 227–242. https://doi.org/10.1016/0031-0182(95)00052-N.
Taylor, K.E., Stouffer, R.J., Meehl, G.A., 2009. A Summary of the CMIP5 Experiment Design. Retrieved from. http://cmip-pcmdi.llnl.gov/cmip5/docs/Taylor_CMIP5_design.pdf.
Tierney, J.E., Pausata, F.S.R., De Menocal, P.B., 2017. Rainfall regimes of the green Sahara. Sci. Adv. 3 (1) https://doi.org/10.1126/sciadv.1601503.
Timmermann, A., Friedrich, T., 2016. Late Pleistocene climate drivers of early human migration. Nature 538 (7623), 92–95. https://doi.org/10.1038/nature19365, 2016 538:7623.
Verseghy, D.L., 2000. The Canadian land surface scheme (CLASS): its history and future. Atmos.-Ocean 38 (1), 1–13. https://doi.org/10.1080/07055900.2000.9649637.
Verseghy, D.L., 2010. The Canadian land surface scheme (CLASS): Its history and future 38 (1), 1–13. https://doi.org/10.1080/07055900.2000.9649637. Http://Dx.Doi.Org/10.1080/07055900.2000.9649637.
Vogel, C.H., Drummond, J.H., 1993. Drought and economic distress: South Africa in the 1800s. Geojournal 30 (1), 93–98. https://doi.org/10.2307/204770.
Wilcoxon, F., 1945. Individual comparisons by ranking methods. Biometrics Bull. 1 (6), 80. https://doi.org/10.2307/3001968.
Wilkins, J., 2021. Homo sapiens origins and evolution in the Kalahari Basin, southern Africa. Evol. Anthropol. Issues News Rev. 30 (5), 327–344. https://doi.org/10.1002/EVAN.21914.
Yu, G., Harrison, S.P., 1996. An evaluation of the simulated water balance of Eurasia and northern Africa at 6000 y BP using lake status data. Clim. Dynam. 12 (11), 723–735. https://doi.org/10.1007/S003820050139/METRICS.
Yuen, K.K., Dixon, W.J., 1973. The approximate behaviour and performance of the two sample trimmed t. Biometrika 60 (2), 369–374. https://doi.org/10.2307/2334550.
Zadra, A., Roch, M., Laroche, S., Charron, M., 2010. The subgrid-scale orographic blocking parametrization of the GEM Model. Atmos.-Ocean 41 (2), 155–170. https://doi.org/10.3137/AO.410204.
Zhang, X., Alexander, L., Hegerl, G.C., Jones, P., Tank, A.K., Peterson, T.C., et al., 2011. Indices for monitoring changes in extremes based on daily temperature and precipitation data. Wiley Interdisciplinary Reviews: Clim. Change 2 (6), 851–870. https://doi.org/10.1002/WCC.147.